



Correlative Organelle Microscopy: Fluorescence Guided Volume Electron Microscopy of Intracellular Processes

Sergey V. Loginov¹, Job Fermie^{1,2}, Jantina Fokkema¹, Alexandra V. Agronskaia¹, Cilia De Heus², Gerhard A. Blab¹, Judith Klumperman², Hans C. Gerritsen¹ and Nalan Liv^{2*}

¹Molecular Biophysics, Debye Institute for Nanomaterials Science, Utrecht University, Utrecht, Netherlands, ²Cell Biology, Center for Molecular Medicine, University Medical Center Utrecht, Utrecht University, Utrecht, Netherlands

OPEN ACCESS

Edited by:

Christopher Guerin,
Vlaams Instituut voor Biotechnologie,
Belgium

Reviewed by:

Sebastian Ludwig V. Munck,
VIB/KU Leuven Center for Brain &
Disease Research, Belgium
Jemima Burden,
University College London,
United Kingdom

*Correspondence:

Nalan Liv
n.liv@umcutrecht.nl

Specialty section:

This article was submitted to
Cell Growth and Division,
a section of the journal
Frontiers in Cell and Developmental
Biology

Received: 06 December 2021

Accepted: 04 March 2022

Published: 11 April 2022

Citation:

Loginov SV, Fermie J, Fokkema J,
Agronskaia AV, De Heus C, Blab GA,
Klumperman J, Gerritsen HC and Liv N
(2022) Correlative Organelle
Microscopy: Fluorescence Guided
Volume Electron Microscopy of
Intracellular Processes.
Front. Cell Dev. Biol. 10:829545.
doi: 10.3389/fcell.2022.829545

Intracellular processes depend on a strict spatial and temporal organization of proteins and organelles. Therefore, directly linking molecular to nanoscale ultrastructural information is crucial in understanding cellular physiology. Volume or three-dimensional (3D) correlative light and electron microscopy (volume-CLEM) holds unique potential to explore cellular physiology at high-resolution ultrastructural detail across cell volumes. However, the application of volume-CLEM is hampered by limitations in throughput and 3D correlation efficiency. In order to address these limitations, we describe a novel pipeline for volume-CLEM that provides high-precision (<100 nm) registration between 3D fluorescence microscopy (FM) and 3D electron microscopy (EM) datasets with significantly increased throughput. Using multi-modal fiducial nanoparticles that remain fluorescent in epoxy resins and a 3D confocal fluorescence microscope integrated into a Focused Ion Beam Scanning Electron Microscope (FIB.SEM), our approach uses FM to target extremely small volumes of even single organelles for imaging in volume EM and obviates the need for post-correlation of big 3D datasets. We extend our targeted volume-CLEM approach to include live-cell imaging, adding information on the motility of intracellular membranes selected for volume-CLEM. We demonstrate the power of our approach by targeted imaging of rare and transient contact sites between the endoplasmic reticulum (ER) and lysosomes within hours rather than days. Our data suggest that extensive ER-lysosome and mitochondria-lysosome interactions restrict lysosome motility, highlighting the unique capabilities of our integrated CLEM pipeline for linking molecular dynamic data to high-resolution ultrastructural detail in 3D.

Keywords: correlative light and electron microscopy, volume electron microscopy, live-cell imaging, lysosome, organelle contact site

1 INTRODUCTION

Eukaryotic cells are compartmentalized in organelles delimited by distinctive intracellular membranes, each with special biochemical functions yet functioning together to maintain cellular homeostasis. Complications in organelle performance are associated with many pathologies ranging from infection, neurodegeneration, and cancer (Wu et al., 2018; Ballabio and Bonifacino, 2019; Ferguson, 2019; Sironi et al., 2020). The next step in understanding cellular regulation is how interconnectivity between different types of organelles is important for function (Gatta and Levine, 2016). This calls for novel microscopy approaches to study spatial and temporal regulation of intracellular processes at the nanoscale level.

Electron microscopy (EM) has immensely contributed to the nanoscale understanding of complex intracellular structure that underlies diverse cellular functions. However, the biggest challenge for EM has been the characteristic lack of 3D information arising from the limited section thickness obtained by classical transmission electron microscopy (TEM). Building on the initial idea of collecting serial TEM or electron tomography (ET) images of consecutive sections to build a 3D volumetric reconstruction (Keene et al., 2008; Knott et al., 2008; Saalfeld et al., 2010), various volume EM approaches have now been developed: scanning EM (SEM) based volumetric approaches; array tomography, in which serial sections from the sample are collected on a substrate (Micheva and Smith, 2007), serial block-face SEM (SBF.SEM), in which the block face is imaged repeatedly after sectioning by an *in situ* ultramicrotome (Denk and Horstmann, 2004), and focused ion beam SEM (FIB.SEM), where an ion beam removes slices from the block face (Heymann et al., 2006). Particularly FIB.SEM, which offers isotropic sub-5 nm resolution in *x*, *y*, and *z*, allows gathering 3D EM information at resolutions able to address many significant biological questions (Bushby et al., 2011; Knott et al., 2011; Lucas et al., 2012; Kizilyaprak et al., 2014; Narayan et al., 2014; Peddie and Collinson, 2014). Volume EM data also open up the possibility of quantitative EM studies without the dimension restriction of 2D EM, by automizing collection of 3D ultrastructural data. Thus, the stage is ready for volume EM to deliver its promise in cell biology (Hoffman et al., 2020), just like confocal fluorescence microscopy (FM) did in the last decades by enhancing our understanding of 3D organization of molecules and organelles within cells.

The unique potential of volume EM is currently limited in throughput as, for each experiment, a relatively large cellular volume is imaged at high resolution. This is incompatible with most life science studies, which often require the analysis of small volumes of several independent samples. If the high-resolution acquisition could be limited to a pre-defined region of interest (ROI), the throughput of volume EM would be considerably enhanced (Burel et al., 2018; Ronchi et al., 2021). With the introduction of correlative light electron microscopy (CLEM), an ROI can be highlighted/selected with FM (a common driver for CLEM). Volume correlative light and electron microscopy (volume-CLEM) approaches offer a unique potential to explore molecular characteristics together with high-resolution ultrastructural details across the cell volume. Recent studies, especially on connectomics, provide very promising examples of volume-CLEM for tissue analysis (Oberti et al., 2011; Collman et al., 2015), for example, by visualizing glia in 3D reconstructions of mouse hippocampal tissue at nanometer resolution (Fang et al., 2018). Moreover, at the cellular level, state-of-the-art volume-CLEM studies visualize protein-ultrastructure relationships in three dimensions across whole cells by identification of morphologically complex structures within the crowded intracellular environment (Hoffman et al., 2020). However, an accurate and reliable correlation between separate 3D-FM and 3D-EM platforms datasets is far from trivial because of the resolution mismatch and the sample transfer in between the two modalities (Ronchi et al., 2021). Current efforts in volume-

CLEM development focus on improving its accuracy, throughput, and accessibility. An integrated CLEM platform (i.e., combining FM and EM in one instrument) inherently resolves this correlation problem as the coordinate planes of the FM-EM are shared. Recently introduced integrated confocal FM and volume EM systems, which can record both confocal fluorescence and reflection images (Brama et al., 2016; Ando et al., 2018), can be used to achieve a robust and streamlined image acquisition. 3D-FM can identify 3D coordinates of ROIs within cells, which can be traced and imaged in volume EM in a targeted way, directly increasing the throughput of the method. Correlation precise enough to target a sub-cellular level ROI (e.g., an organelle) in 3D is specifically challenging and has thus far not been demonstrated.

Understanding intracellular processes (e.g., organelle interconnectivity) ultimately requires linking molecular and dynamic information from live cells to a high-resolution ultrastructure. Therefore, a next major step forward in volume EM will be to correlate EM data to functional information from (live-cell) FM (Blazques-Llorca et al., 2015; Hoffman et al., 2020). We and others have shown that linking functional or dynamic information obtained with live-cell imaging to the underlying fine structure of the cell opens up powerful possibilities to study mechanistic processes with respect to their ultrastructure (Russell et al., 2016; Collinson et al., 2017; Fermie et al., 2018). Correlation with live-cell FM also aids the identification and capture of rare cellular structures or events, which is very challenging, time demanding, and at times basically impossible without smart tracking for EM imaging (Burel et al., 2018; Delpiano et al., 2018). An integrated CLEM platform fulfills these requirements by enabling a direct translation between live-cell FM and volume EM and the targeting identified live-cell events for follow-up ultrastructural imaging. Therefore, an FM-guided imaging pipeline for volume EM data collection is essential to improve the efficiency, throughput, and quantitative capabilities of the technique.

We present an optimized imaging pipeline to identify and target single organelles for volume-CLEM within the complex cellular environment. Following live-cell FM and fixation, we prepare cells for volume EM imaging. We then use confocal laser scanning microscopy integrated into a FIB.SEM to quickly and accurately retrace single endo-lysosomes in the complete sample and generate the corresponding 3D volume EM dataset. With this pipeline, we correlate motile characteristics of targeted organelles to their morphology, yielding essential information on their identity and cellular surroundings, such as the number and types of contact sites with the endoplasmic reticulum (ER).

2 MATERIALS AND METHODS

2.1 Cell Culture

HeLa cells were cultured in a 37°C, 5% CO₂ incubator, in T75 culture bottles (Corning). Cells were maintained in Dulbecco's Modified Eagle's Medium (DMEM; Gibco) supplemented with 10% fetal bovine serum, 2 mM L-glutamine, 100 U/ml penicillin, and 100 µg/ml streptomycin (referred to as complete DMEM). Cells were passaged when confluency reached 85%–90%.

For CLEM, HeLa cells were grown on gridded glass coverslips, prepared as described earlier (Fermie et al., 2018). On the next day following seeding, the cells were transiently transfected with a construct encoding mEmerald-Sec61b-C1 (Nixon-Abell et al., 2016), which was a gift from Jennifer Lippincott-Schwartz (Addgene plasmid # 90992), for 16 h. Transfections were performed using Effectene transfection reagent (Qiagen) according to the manufacturer's instructions. Prior to FM, cells were incubated with fiducial markers (Fokkema et al., 2018) at a concentration of 1 $\mu\text{g}/\text{ml}$ and cell-permeable lysosome stain SiR-Lysosome (SpiroChrome) at a concentration of 0.5 μM in complete DMEM and incubated for 3 h.

2.2 Fluorescence Microscopy

Live imaging was performed on a Deltavision RT widefield microscope (GE Healthcare) equipped with a conditioned imaging chamber set to 37°C and 5% CO₂. Time-lapse imaging was performed using a $\times 100/1.4$ numerical aperture (NA) oil immersion objective, and images were recorded on a Cascade II EM-CCD camera (Photometrics). Live-cell imaging was performed for 3–5 min, after which the cells were fixed *in situ* by adding 1 ml of fixative containing 4% paraformaldehyde (Sigma) and 0.05% glutaraldehyde (25% solution in dH₂O, Merck) in 1 \times PHEM buffer (60 mM PIPES, 25 mM HEPES, 10 mM EGTA, 2 mM MgCl₂, pH = 6.9) to the imaging holder with the camera still active, to obtain images until the cells are fixed. After fixation, a Z-stack was recorded for all fluorophores using a Zeiss LSM700 CLSM equipped with $\times 63/1.4$ NA oil immersion objective. Z-stacks were collected with a 200 nm step size. The position of cells relative to the grid of the coverslips was recorded using polarized light.

2.3 Sample Preparation for Volume EM

Cells were prepared for electron microscopy according to a protocol described earlier, with minor modifications (van Donselaar et al., 2018). Briefly, samples were postfixated using 1% osmium tetroxide (w/v) with 1.5% potassium ferrocyanide (w/v) for 1 h on ice, incubated with 1% thiocarbohydrazide in dH₂O (w/v) for 15 min, followed by 1% osmium tetroxide in dH₂O for 30 min. Samples were EM stained with 2% uranyl acetate in dH₂O for 30 min and stained with Walton's lead aspartate for 30 min at 60°C. Dehydration was performed using a graded ethanol series. Samples were embedded in Spurr resin and polymerized for 48–60 h at 65°C following the extremely thin layer plastification method (van Donselaar et al., 2018). Resin embedded samples on the glass coverslips were subsequently coated with 8 nm carbon and carbon-tape mounted on aluminum stubs.

2.4 Electron Microscopy

A Scios FIB.SEM (ThermoFisher) was used. It included an Everhart-Thornley Detector (ETD), an in-lens detector of backscattered electrons (BSE), and an in-the-column detector of secondary electrons (SE). The ETD was used for imaging of sample surfaces. The BSE detector was used for imaging cellular ultrastructure in 3D. The in-the-column SE detector was used to

enhance fiducial marker contrast. The FIB was equipped with a Ga-ion source; for the 3D acquisition, a current of 0.4 nA and an acceleration voltage of 30 kV were used. The 3D acquisition in the FIB.SEM was controlled by the Slice&View software version 3 (Thermo Fischer).

2.5 Integrated Confocal Laser Scanning Microscope

The integrated CLSM was equipped with a Nikon industrial inspection objective lens (ELWD series, Plan Apo 100x NA0.9). A lens of focal length 120 mm (25 mm diameter, OptoSigma anti-reflection coated doublet lens DLB-25–120 p.m.) was used as a tube lens. For lateral optical scanning, a Yanus scan head (FEI Munich) equipped with a 50 mm focal length scan lens was used. As an excitation source, a 532 nm laser (Omicron, integrated with an Acoustic Optical Modulator in LightHUB housing) coupled *via* a single-mode optical fiber was used. The excitation and detection light paths were combined inside the scanning head *via* a dichroic mirror (T560lpxr-UF2, Chroma). The detected light was coupled into a multi-mode fiber (FG010LDA, Thorlabs) with a core diameter of 10 μm (about 1 Airy disk). The light from the sample was split by a second dichroic mirror (T565LP, Chroma) into fluorescence and reflection parts. Backreflected light was detected by a PMT operating in current mode (PMMA01, Thorlabs). After bandpass filtering (ET585pxr-65, Chroma), the fluorescence signal was detected by a photon-counting PMT (H7422P-40, Hamamatsu). For sub-micrometer axial scanning, a single axis piezo-stage (E-601.1SL, Physik Instrumente) was mounted on top of the FIB.SEM stage. iCLSM was controlled *via* a National Instruments NI-6251 DAQ card using LabView software. The LabView codes can be found at https://github.com/UUtrechtTT/integrated_CLSM_control_software_LabView. See also **Supplementary Figure S1** for the iCLSM/FIB.SEM setup.

2.6 Integrated Confocal Laser Scanning Microscope and FIB.SEM Pipeline

Initially, a low magnification, low-exposure SEM image was acquired to find the main grid markings (numbers and letters). Using those markings, the square where the live-cell imaging was performed was found. Another low-exposure SEM image ("snapshot" at the current of 10 pA, dwell time 0.5 μs , and pixel size of $\sim 250 \times 250 \text{ nm}^2$) was taken of the suspected square to verify that the correct cells were found. Performing these steps using SEM has an advantage because of the much wider field of view of SEM compared to that of the integrated CLSM (up to 350 μm) and the large depth-of-focus of the SEM. However, the topographical contrast of the SEM is much lower than of the reflection light channel of the integrated CLSM. The SEM exposure of the sample should be minimized as much as possible because the fluorescence quenches strongly under electron radiation. In the next step, the sample was transferred under the integrated CLSM. Herein, we made overview images with pixel size larger than 0.5 μm and a dwell time of 3 μs . In the reflected light channel, we can find the cells and refine the Z position of the sample. The shape of the cell is

then used to find ROI from the live-cell/fixed cell images. Next, we take a fine-resolution image ($34 \times 34 \text{ nm}^2$ pixels, Z step of 100 nm and dwell time of 24 μs) of cell area of $35 \times 35 \mu\text{m}^2$ or smaller. In the fluorescence channel in the acquired image, some of the nanofiducial particles were visible. Their configuration allowed refining the position of the ROI relative to the surface features detected with the reflection light channel. All ROIs selected in the live-cell data were recorded in the same manner with the integrated CLSM. Next, the sample was transferred back under the FIB/SEM. At this step, the surface features of the cells were accurately studied in SEM with a pixel size of $17 \times 17 \text{ nm}$ and dwell time of 1 μs and beam current of 50 pA because fluorescence quenching had become of no issue after the integrated CLSM imaging was performed. The surface features of the cell recorded at this step were used to refine the ROI in the SEM field of view and determine the acquisition volumes of the FIB/SEM itself.

2.7 Alignment of FIB/SEM Data

The raw SEM images of 3D FIB/SEM data were aligned using MATLAB (see https://github.com/UUtrechTT/Slice_and_View_postprocessing_code_MatLab). The vertical alignment (y -axis in SEM images, z -axis in the original orientation) was performed *via* the detection of the glass substrate in the SEM images. The alignment in the X direction was performed using the correlation of consecutive images. The height of XY slices is calculated relative to the substrate level.

2.8 Correlation/Targeted Imaging Routine

In the live-cell data, the ER and the lysosomes are used to define the region of interest. After fixation, a CLSM image is collected of the same lysosomes and the ER and, additionally, the fiducial particles emitting in another channel. The shape of the cell visible in SEM and the ER configuration can be used for correlation. The fluorescence of the nanoparticles is visible in the integrated CLSM and allows for registration with the non-integrated CLSM. The fluorescence channel of integrated CLSM is directly linked with the reflection channel of the integrated CLSM. In the reflected light channel, the cell shape and cell topography are visible in fine detail. The same fine details (i.e., slopes, protrusions, and bumps) are visible in the reflection light channel of the integrated CLSM and the SEM image. These fine details can be used for the fine registration between these two (vacuum) modalities. Thus, the accurate finding of the ROI in the FIB/SEM relies on the following ladder of registration steps: from the fiducials in the non-integrated CLSM to the fiducials visible in the integrated CLSM. Next, the fiducials in the CLSM can be related exactly to the surface features of the cell, with are also visible in the SEM, albeit with different contrast.

2.9 Image Correlation, Analysis, and Segmentation

Registration of 3D CLSM and 3D FIB/SEM data was achieved by the following steps: first, 2D maximum intensity projection of CLSM data and 2D maximum intensity projection of integrated CLSM data were registered manually to find relative rotation angle. The registration was based on the clusters of fluorescent nanoparticles. Next, the whole 3D CLSM data were rotated

around the z -axis by the angle found at the first step. Then, the sub-volume of 3D CLSM enclosing the ROI was copied with a several-pixel margin. Afterward, the sub-volume was interpolated to a smaller voxel size using the bilinear algorithm. The 3D FIB/SEM data were reordered to match those of CLSM data (the native orientation in Slice&View software is XZY), and voxel dimensions were equalized: binned along X and Z directions (SEM scanning directions) and interpolated along Y direction (FIB slicing direction). The voxel sizes matched those of the 3D CLSM data sub-volume at the previous step. Finally, the correct sub-volume of 3D CLSM data was selected manually, and the 3D FIB/SEM data were added to it as a fourth color channel.

We employed a semi-automated approach of the custom-written MATLAB code (see https://github.com/UUtrechTT/Slice_and_View_postprocessing_code_MatLab) for segmentation of the 3D FIB/SEM datasets. The segmentation was performed consequently for each type of cell compartments. At first, the lysosomes were segmented. Then, the voxels of the lysosome were zeroed in the volume, and the segmentation was performed for the mitochondria (if any were present in the volume). As the last step, the ER segmentation was performed with all the previously segmented organelles zeroed in the volume.

The semi-automated segmentation “in bunches” was performed in the following manner. For every 10 2D slices, the average image (i.e., “bunched slices”) was shown to the user. Then, the user drew a contour around the suspected organelle, which defined the area where the automated segmentation would be performed. All automated steps were performed on a 2D basis using the standard MATLAB Image Processing Toolbox functions. Otsu thresholding was performed (two levels in the case of lysosome and three levels in other cases) in the user-selected area of the averaged image. The highest level obtained from the Otsu algorithm was used for thresholding the suspect area of each of the substitute original slices of the stack. The images were then subjected to Canny edge detection, and the edges were morphologically filled. The automated steps were parallelized for the slices of the bunch. After the automated steps were performed, the new averaged image was shown to the user with zeroed detected areas. At this step, the user could define another area where the organelle was visible or accept the results of the automated steps and proceed to process the next bunch of the slices.

For each organelle, the segmentation procedure was performed three times along three main axes of the stack (for XY, XZ, and ZY slices). A pixel was considered belonging to the organelle if detected in any of the two steps.

3 RESULTS

3.1 Correlative Organelle Microscopy Workflow: Deep Sub-Cellular Precision Volume-CLEM Using Integrated 3D CLSM and FIB/SEM

Correlating single organelle-sized, intracellular regions-of-interest (ROIs) from fluorescence (FM) to electron microscopy (EM) is challenging due to the limited resolution of FM, the

inherently different contrast mechanisms of the two modalities, and the highly crowded content of the cell (Ando et al., 2018). These challenges are amplified when correlating 3D FM to 3D EM images and even further when using live-cell imaging as an FM method. Integrated CLEM instruments (with the LM built in the EM) greatly facilitate retracing the ROI from FM to EM (Liv et al., 2013; Koning et al., 2019) as the coordinate systems of the FM-EM are shared. Recently, multiple integrated (confocal) FM and volume EM systems were reported (Brama et al., 2016; Ando et al., 2018; Delpiano et al., 2018; Gorelick et al., 2019; Lane et al., 2019). We add to this a home-built system integrating a Confocal Laser Scanning Microscope (CLSM) into a Focused Ion Beam Scanning Electron Microscope (FIB.SEM), similar in geometry to a previously reported (Timmermans et al., 2016) integrated system, as outlined in **Supplementary Figure S1**. In short, the CLSM unit is mounted on one of the side ports of the FIB.SEM chamber. The FIB.SEM and CLSM image the sample from the same direction, while switching between the two modalities is simply accomplished by shuttling the specimen on the accurate motorized stage. The integrated CLSM (iCLSM) is equipped with a Nikon industrial inspection objective lens (ELWD series, Plan Apo 100x NA0.9).

3.1.1 Endocytic Fiducials for Improved 3D Correlation

Even in such an integrated CLEM platform, the accuracy of FM-EM registration/correlation is limited by FM resolution, especially in the z-dimension. Several organelles can be located within the same fluorescent spot, causing the risk of misidentification. We tackled this problem by adding gold core silica shell fiducials to cells prior to imaging. These fiducials, recently developed in our labs (Fokkema et al., 2018; Mohammadian et al., 2019), are visible and highly compatible with live-cell imaging. They are taken up by endocytosis, which generates a natural 3D distribution within the cell throughout the endo-lysosomal system (Fokkema et al., 2018; Prabhakar et al., 2020). The resulting array of well-distributed puncta provides an accurate 3D translation map between FM and EM and enables the identification and registration of even single organelles. Moreover, their fluorescence is retained after osmium fixation and serves as suitable anchors for the translation of coordinate systems between stand-alone CLSM, iCLSM, and volume EM.

We then set up the following high accuracy, live-cell volume-CLEM pipeline consisting of the steps: 1—image live cells in a stand-alone FM, 2—fix cells and make a confocal Z-stack, 3—prepare cells for FIB.SEM, 4—place and image the sample in the integrated platform-map confocal Z-stack to 3D iCLSM image, 5—target and image the pre-identified region in FIB.SEM. An outline of this high accuracy live-cell volume-CLEM workflow is shown in **Figure 1**, and detailed in **Supplementary Figure S2**.

3.1.2 Fluorescent Microscopy: From Live-Cells to 3D Confocal Z-Stacks

To demonstrate our approach, we labeled live HeLa cells for two distinct organelles; endoplasmic reticulum (ER) and lysosomes. Cells were cultured on gridded glass coverslips with etched marks (Polishchuk et al., 2000) and transiently transfected (16 h) with mEmerald-Sec61 β , localizing to ER membranes. Then, the

transfection medium was replaced with a medium containing SiR-lysosome (SiRLyso) (Lukinavičius et al., 2016), marking functionally active lysosomes and containing the above introduced endocytic fiducial nanoparticles, both for 3 h at 37°C. To view the dynamics of ER and lysosomes and their interactions, we performed live-cell imaging of individual fluorescent organelles. We recorded the mEmerald (ex/em 487/509 nm) and the SiRLyso (ex/em 652/674 nm) channels with 1s/frame over 2–3 min (**Figure 1A**). Then, cells were fixed *in situ* on the microscope stage by adding fixative directly in the imaging chamber. This assures no imaging gap between the last live-cell frame and the corresponding image after fixation. Following fixation, fluorescent confocal Z-stacks were recorded of the same cell capturing the 3D distribution of mEmerald-Sec61 β , SiRLyso, and the fiducial particles (ex/em 543/576 nm). **Figure 1B** shows a maximum intensity projection of the Z-stack; fiducial particles (green), ER (blue), and lysosomes (red) are visible. With the confocal Z-stack, the exact *x-y-z* coordinates of ER and lysosomes are visualized with respect to the fiducial markers (**Figure 1C**).

3.1.3 Relocating the Region of Interest in FIB.SEM Using iCLSM

Samples were removed from the microscope stage, postfixed, with osmium-thiocarbohydrazide-osmium (R-OTO), and further stained with uranyl acetate and Walton's lead aspartate. Cells were embedded in resin following the “extremely thin layer plastification” (ETLP) method (van Donselaar et al., 2018). For a more in-depth description of these protocols, we refer to **Section 2**. After resin embedding, the cells were coated with carbon, mounted on a stub, and transferred to the integrated CLSM/FIB.SEM setup operating under high-vacuum (see **Supplementary Figure S1**). A quick re-localization of the cells imaged previously in the stand-alone CLSM was achieved using the SEM to show the markings on the coverslips (**Figures 1D–F**). Interference reflection contrast mode of iCLSM (Weber, 2003) can resolve some features of the cell (e.g., cellular contours) and allows easy correlation between the CLSM to find back the cells (**Figure 1E**). The interference contrast images expose various surface topology features of the cells. As many of these features are also visible in the SEM images, this registration generates a first 2D correlation map around the ROI (red rectangle in **Figures 1B,E**). Then, the confocal fluorescence image from iCLSM localizes fiducial nanoparticles (which notably retain their fluorescence in the epoxy resin) in *x*, *y*, and *z* (**Figure 1F**). iCLSM image of the fiducial particles directly matches the fiducial channel in the CLSM image collected before EM sample preparation (note the correspondence in **Figures 1C,F**) and provides a 3D translation anchor. After this, we could reliably start the 3D FIB.SEM acquisition of this targeted ROI.

3.1.4 Volume EM Imaging and 3D Correlation

In FIB.SEM, samples are imaged by scanning the surface of an ROI using the electron beam, after which a thin layer is ablated from the surface using the FIB (**Figure 1G**). This cycle is repeated until the ROI has been imaged, allowing a 3D reconstruction of the sample. We performed the slice-by-slice acquisition both with

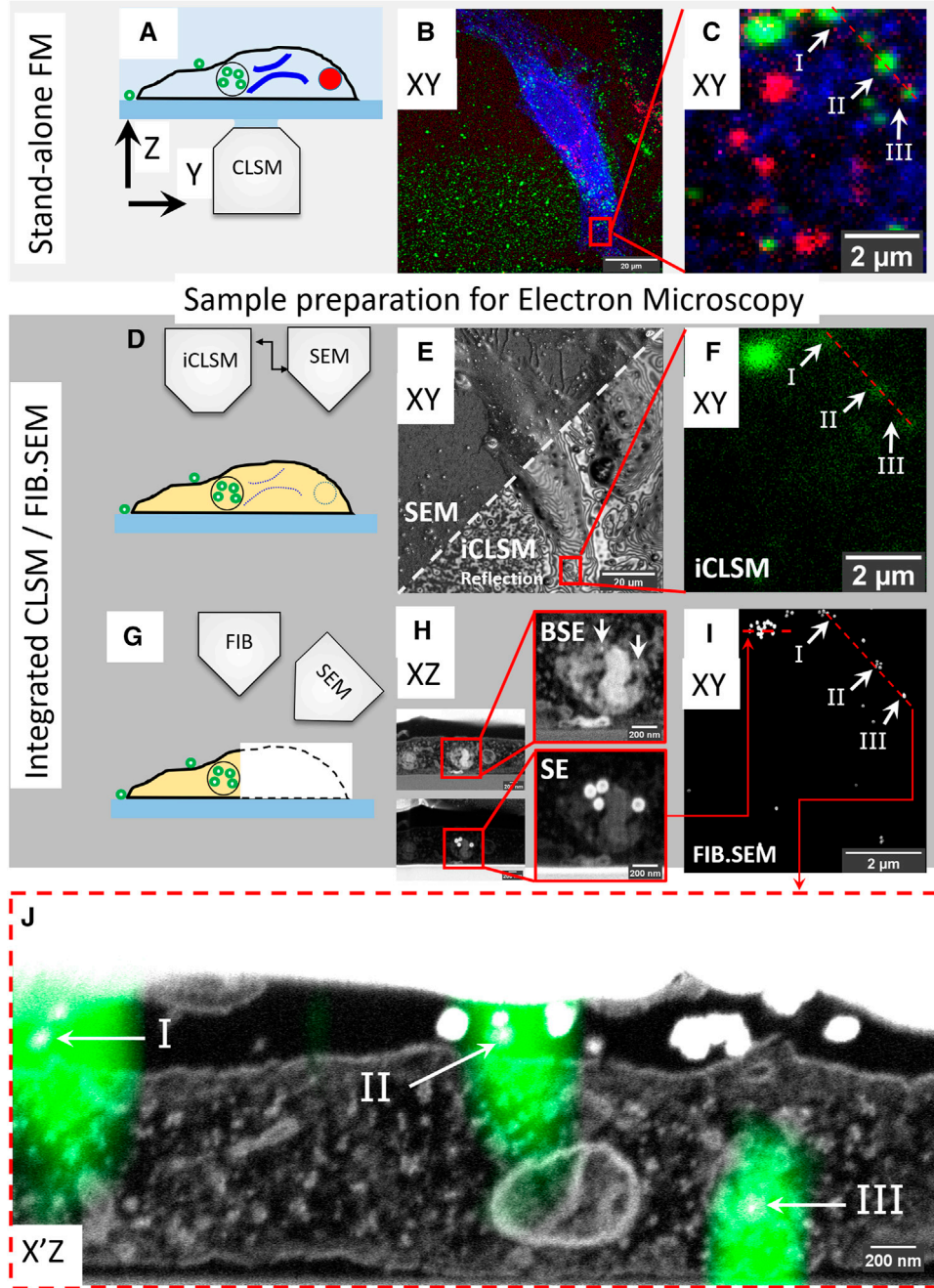


FIGURE 1 | High accuracy 3D correlation workflow from live-cell-to-volume EM with iCLSM. **(A–C)** Live-cell imaging and CLSM. **(A)** Live-cell imaging of cells on gridded coverslips in stand-alone CLSM followed by z-stack recording of fixed cells. **(B)** Maximum intensity projection of the CLSM Z-stack. ER (blue), active lysosomes (red), and endocytic fiducial particles (green). **(C)** The selected ROI, red square, within the cell in **(B)**. **(D–F)** Correlation with iCLSM. **(D)** Locating the ROI in the FIB-SEM chamber by iCLSM after EM preparation. **(E)** Reflection mode imaging in iCLSM to navigate through the gridded glass coverslip and fast-tracking of ROI by cell shape. iCLSM reflection image (lower half) relates easily with SEM (upper half). **(F)** The ROI can be localized by the fluorescence mode of iCLSM. The (remaining) fluorescence signal of the fiducial nanoparticles is used for correlation back to the CLSM image in **(C)**. **(G–I)** 3D FIB-SEM acquisition of the re-established ROI. **(H)** Slice-by-slice acquisition is performed with backscattered electrons (BSE, top) and secondary electrons (SE, bottom). Fiducial nanoparticles have a clear signature of a bright backscattering core (top) and shell in secondary electrons (bottom). **(I)** They can be thus filtered from the acquired data stack to aid precise correlation of ROI between CLSM and FIB-SEM. Note the one-to-one correspondence between panels **(C,F,I)**. **(J)** Overlay of 3D CLSM data from the fixed cell and the 3D FIB/SEM data. EM image corresponds to the plane of red dashed line in **(C,F,I)**.

backscattered electrons (BSE) (**Figure 1H**, top) and secondary electrons (SE) (**Figure 1H**, bottom). Fiducial nanoparticles have a clear signature, with a bright backscattering by both the gold core and a bright secondary electron emission by the silica shell, which improves their visibility and makes them well-suited for FIB.SEM image acquisition. The fiducial nanoparticles are found in endolysosomal compartments and can be detected at an individual particle level (**Figure 1H**). With the high resolution provided by FIB.SEM in x , y , and z dimensions, single particles can be identified and fitted to the fluorescence Z-stack data (**Figure 1J**). Using the fiducials, we correlated and registered the 3D CLSM data from the fixed cell with the 3D FIB.SEM dataset (**Figures 1I,J**, also see 3D-overlay **Supplementary Video S1**). **Figure 1J** shows the reconstructed EM image corresponding to the dashed line in the FM images in **Figures 1C,F**. The fluorescent spots I and II shown with arrows point to fiducials outside the cell and III to intracellular fiducials in an endosome. We show a correlation accuracy at the level of single, 90 nm sized nanoparticles, which is far below the x , y , z resolution limits of the FM and allows studying sub-organelle structures.

3.2 Correlation of Organelle Motility and Function to Morphology by Targeted Volume-CLEM

Next, we utilized our high-precision, live-cell-to-volume-CLEM pipeline to link the dynamic behavior of single, active endolysosomes to their morphology and neighboring environment at nanometer resolution. Besides motility, live-cell imaging was used to analyze functional characteristics of organelles, exploiting fluorescent reporter probes. As an example, we used the SiRLyso probe to report the activity state of lysosomal hydrolase cathepsin D in single lysosomes (Butkevich et al., 2017). In a previous 3D CLEM study (Fermie et al., 2018), we used a constellation pattern of at least three fluorescent spots found by live-cell imaging to retrace a similar pattern of endosomal organelles in the volume EM data. Although this proved a powerful approach, the correlation of 3D FM and 3D EM data by matching the organelle constellations was relatively time-consuming and limited in accuracy. With our current approach, the correlation of the fiducial signal between the pre-embedding CLSM z-stack and post-embedding iCLSM assures that we know the exact z-plane of each organelle imaged in live-cell FM. Moreover, our correlation is not limited to organelles bearing fiducial particles but extends to all fluorescent signals, even when lost after EM embedding, using the fluorescence signal from fiducial particles as an anchor in translating data to volume EM. Hence, we can correlate each live-cell imaged organelle to the volume EM data (see **Supplementary Figure S2**). This significantly eliminates the time and computational need for correlation of matching organelle constellations between datasets and hence notably increases the throughput (e.g., organelles analyzed per cell) of the live-cell CLEM workflow.

Live-cell imaging allows studying key temporal, functional (e.g., pH and hydrolase activity as we show here), and structural parameters of single organelles over an extended period of time,

and by 3D CLEM, we correlate these directly to nanometer architecture, cellular context, and inter-organelle connections. As a proof of principle, **Figure 2** shows the correlation sequence from a live-cell movie of hydrolase active lysosomes and ER to volume EM. For live-cell imaging (**Figure 2A**), we recorded SiRLyso (lysosomes) and Sec61 β (ER) channels in a single focal plane to reach the temporal resolution required to visualize transient events on a sub-second scale (<1 s between frames, see live-cell **Supplementary Video S2**). We analyzed 14 lysosomes (SiRLyso positive organelles) for their dynamic behaviors, such as speed, displacement, fusion, or interaction with other lysosomes and ER (**Figure 2B**). We then fixed cells *in situ* by adding fixative directly to the medium in the live-cell holder, while the camera was still acquiring images (**Figure 2C**). In the fixed material, Z-stacks of the ROI were recorded to visualize SiRLyso, Sec61 β , and fiducial particles (**Figure 2C**). The samples were prepared for EM and imaged following the routine explained in the previous section and **Figure 1**. With the ultrastructural resolution of EM, we analyzed compartment identity, fusion profiles with other compartments, interactions with surrounding structures, and inter-organelle interactions. Finally, we integrated the multi-modal data collected per organelle, from live-cell imaging to 3D-EM (see 3D-overlay **Supplementary Video S1**).

The movies defined lysosome#1 as the most stable organelle of the whole set. It shows no displacement within 3 min, and its velocity is fixed at 0.07 $\mu\text{m/s}$, resembling the Brownian motion in a confined area. Lysosomes are heterologous in shape and, by EM, can be classified by morphological characteristics such as size and shape, as well as electron density and contours of their content (Meel and Klumperman, 2008; Fermie et al., 2018). The EM data identified lysosome#1 as an (auto)lysosome, showing a heterogeneous content with an electron-dense region and irregularly organized internal membranes. Its size is $0.71 \times 0.69 \times 0.74 \mu\text{m}$. Intriguingly, this stable lysosome has extensive contact sites, covering two-thirds of its surface area, both with mitochondria and ER. Especially its interaction with the mitochondria wrapping it from three sides over a $2 \mu\text{m}^2$ contact area creates a very confined space (**Figures 2D,E**).

In contrast to lysosome#1, lysosome#4 was very motile with an average velocity of 0.2 $\mu\text{m/s}$, traveling over a distance of 2.8 μm in 3 min before it reached the final position also visualized in EM. The organelle first exhibits directional movement toward ($\sim 100^\circ$) the nucleus and then meets lysosome#3 (which is quite stable until the meeting point) at 150s, after which they together move directionally toward ($\sim 270^\circ$) the plasma membrane (see live-cell **Supplementary Video S2**). The directional and stable trafficking characteristics indicate that lysosome#3 and lysosome#4 are transported *via* microtubules and associated motors. The size of lysosome#3 is $0.43 \times 0.61 \times 0.51 \mu\text{m}$ and, by EM, it shows a heterogeneous dense lumen. On the contrary, lysosome #4, with a size of $0.39 \times 0.77 \times 0.54 \mu\text{m}$, has a relatively electron-lucent lumen compared to lysosomes#1 and #3, with irregularly organized internal membranes and numerous intraluminal vesicles (ILVs) (**Figures 2D–F**). In contrast to lysosome#1, lysosome#3 and lysosome#4 do not display contact sites with mitochondria and are not wrapped by ER cisternae. Rather, they

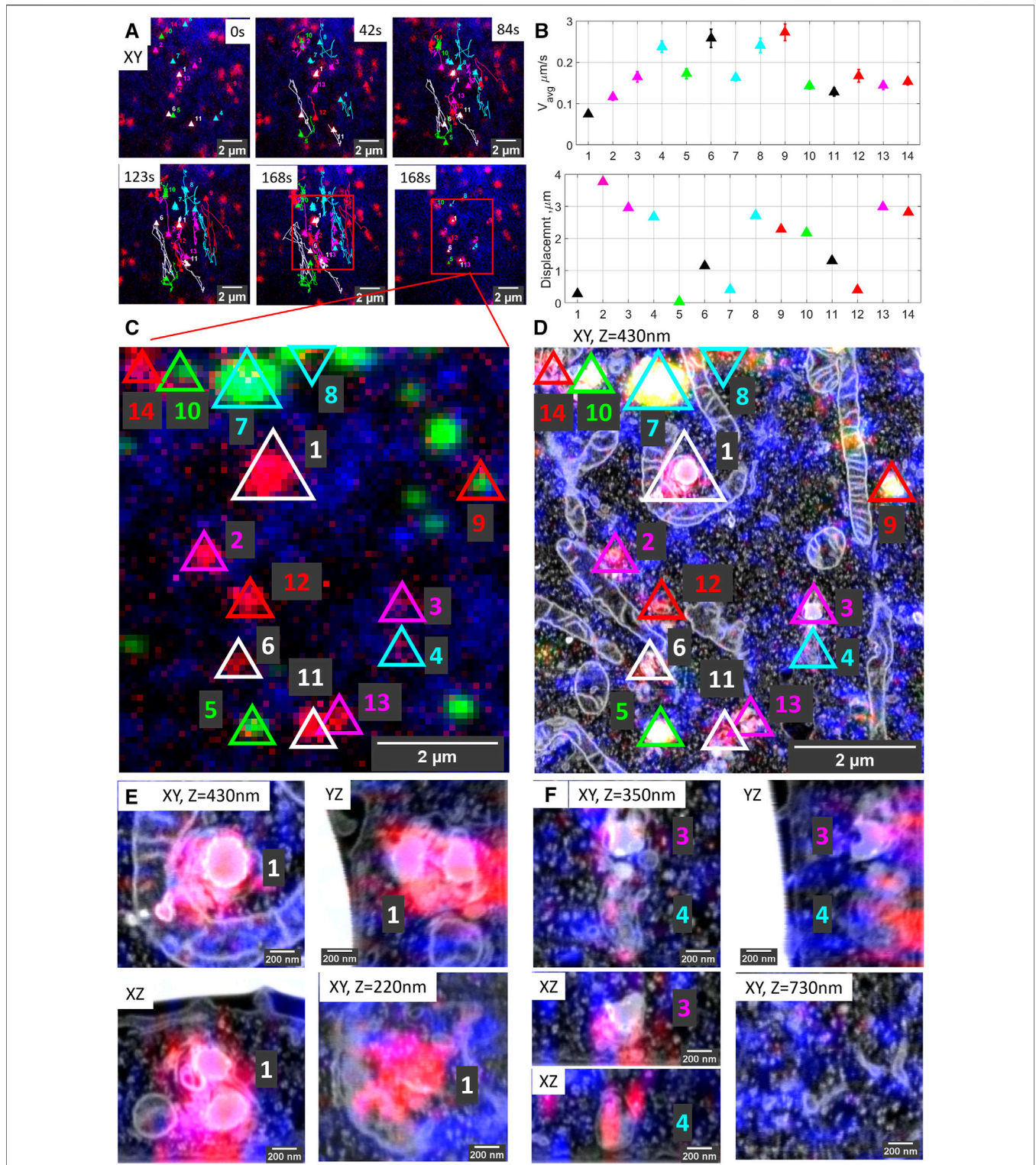


FIGURE 2 | Organelle dynamics directly correlated to morphology. **(A)** Time-lapse images from live-cell imaging. Lysosomes are stained with SiRLyso (red) and ER with mEmerald-Sec61β (blue), and the cells have endocytosed fiducial particles (green). We selected 14 SiRLyso positive, enzymatically active lysosomes and traced their dynamic behavior over 3 min. **(B)** Plot of the average velocity ($\mu\text{m/s}$) and total displacement of each selected organelle, numbered from lysosome#1 to lysosome#14 in the x-axis. For example, lysosome#1 is very static, whereas lysosome#4 moves fast over extended distances. **(C)** Max intensity projection of CLSM stack recorded on the same cell after fixation. Fiducial markers are visible in green. Each identified and analyzed organelle is numbered as in **(B)**. **(D)** Following live-cell imaging and CLSM, cells are prepared for EM, imaged, and high-precision correlation is achieved using iCLSM-FIB-SEM. **(E)** Higher magnification images of lysosome#1, lysosome#3, and lysosome#4 display their distinct morphologies from different planes and interaction with surrounding cellular organelles. See supplementary data for the rest of the lysosomes.

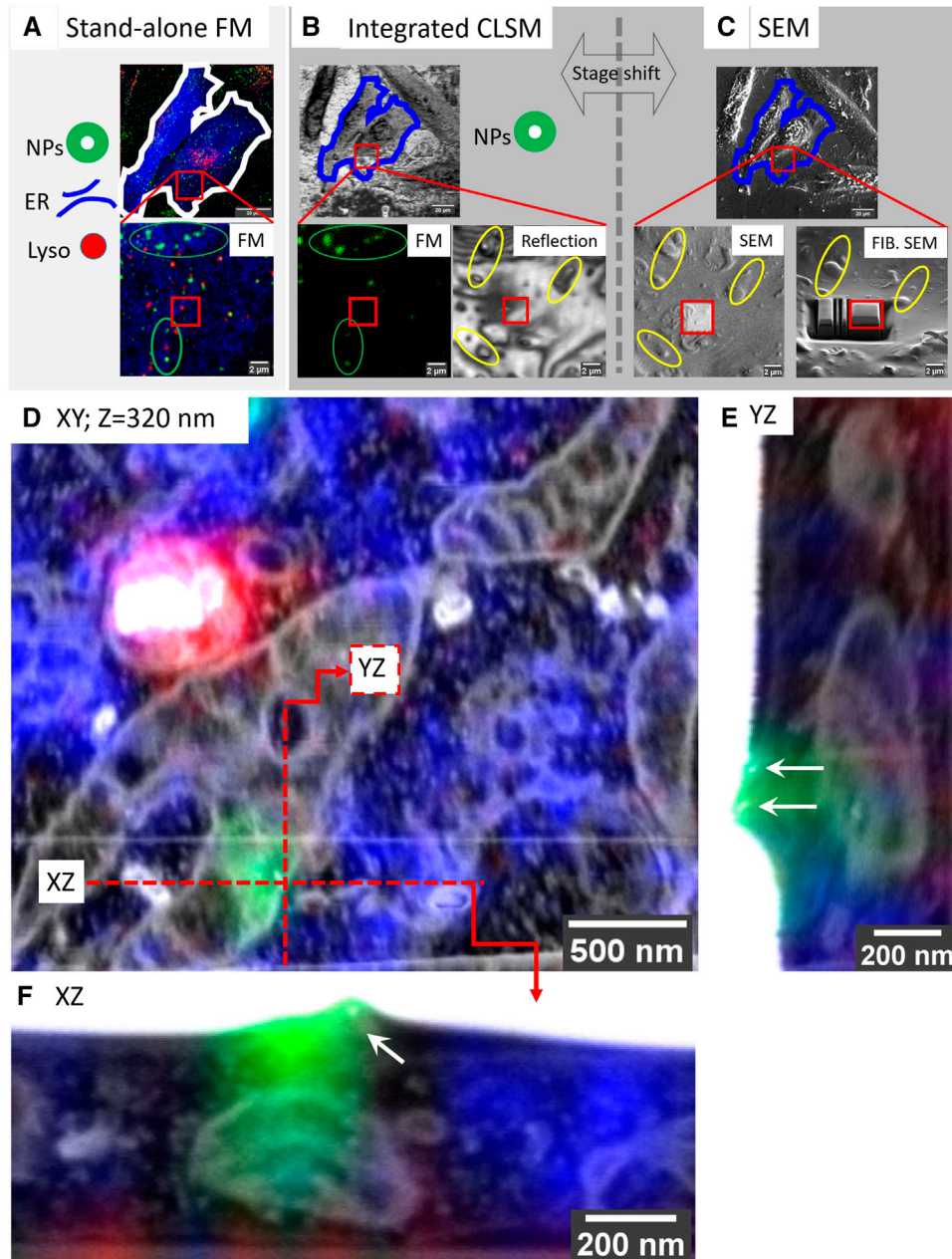


FIGURE 3 | Targeted imaging of minimized volumes in FIB-SEM using iCLSM. **(A–C)** High-accuracy correlation routine for targeted imaging in FIB-SEM. **(A)** Maximum intensity projection of a confocal z-stack collected at CLSM from fixed cells, following optional live-cell imaging. 3D CLSM data show ER (mEmerald-Sec61β, blue), lysosomes (SiRlyso, red), and endocytic fiducials (green). Red square indicates the ROI bearing a single lysosome selected for targeted volume EM. **(B)** The cells and the ROI are traced back after EM sample preparation. Fluorescence of endocytic fiducials is visualized by iCLSM and correlated to the CLSM data (green ellipses), providing the coordinates of the ROI, even when the ROI itself has no fiducial particles. Reflection image collected by iCLSM provides topographic information correlated with SEM for fine alignment (yellow ellipses). **(C)** Once precisely located, the Pt layer is deposited to protect the ROI from FIB, and trenches are prepared for imaging only the small ROI area. **(D)** The small ROI, bearing a single lysosome not reached by endocytic fiducial particles, is targeted and imaged in FIB-SEM. 3D CLSM data, ER, lysosomes, and endocytic fiducials, are overlaid with the 3D FIB-SEM data. **(E,F)** Two fiducial particles located on the plasma membrane are used as a blind target to assess correlation/targeting efficiency. Green fluorescence signal of the particles is correlated to their gold core with an accuracy of 60 nm in X **(E)**, 90 nm in Y **(F)**, and 330 nm in Z.

only touch the ER at 2 and 3 points, respectively. As also reported by others (Cabukusta and Neeffes, 2018; Wong et al., 2019), these data indicate that interactions of lysosomes with other organelles

have a defining role in their motile characteristics. Our high accuracy live-cell volume-CLEM workflow provides a unique means to mechanistically study these interactions. For further

analysis of the organelles in this ROI, see **Supplementary Figure S3**. Note that 10 out of the 14 organelles correlated and analyzed in the ROI have no fiducial particles.

3.3 Rapid Volume-CLEM of Targeted Subcellular Region of Interest With <100 nm Accuracy

The possibility of matching all coordinate planes between 3D-FM and 3D-EM modalities allows us to address a major bottleneck in volume EM approaches: the throughput. In most volume EM imaging techniques, especially in FIB-SEM, hitting the ROI within the imaging volume is ensured by maximizing the image area. This imposes a compromise between long imaging durations (days to weeks) and resolution (low to high). Herein, we tackle this problem using iCLSM to reliably identify and select a very confined ROI (e.g., a single lysosome) for volume EM data collection. Using this targeted approach, we lower the imaging time for a selected ROI from several days to 1–2 h.

To demonstrate the power of the targeted imaging approach in **Figure 3**, we selected a very small ROI of a single SiRLyso positive lysosome devoid of fiducial particles (**Figures 3A,B**, red square) for volume EM. The CLSM—iCLSM correlation provides an accurate 3D map between FM and EM and delivers the 3D coordinates of all organelles within the complete block using the endocytic fiducials in the surrounding organelles as an anchor, including the selected organelle without fiducial particles (e.g., the red labeled lysosomes in **Figure 3A** are not visible in **Figure 3B**). Because the x , y , and z coordinates of the identified organelles are exactly known a priori, only a very small volume needs to be imaged in FIB-SEM. This greatly minimizes the time spent on pre-imaging procedures (i.e., trench milling and Pt layer deposition, **Figure 3C**), as well as the actual image acquisition. Hence, the targeted lysosome was visualized in 3D within only ~2.5 h in FIB-SEM (with voxels of $1.2 \times 1.2 \times 10$ nm and dwell time of 3 μ s), by direct correlation with the corresponding FM data (**Figure 3D**; **Supplementary Video S3**). The CLEM data show, by FM, that the selected organelle is positive for active cathepsin D (SiRLyso signal) and not reached by endocytosed fiducial particles. By EM, we confirm the absence of fiducial particles and show that the lysosome has an electron-dense lumen with clearly degraded content, a spherical shape with an approximate diameter of 560 nm, and extensive contact sites with ER and mitochondria.

To measure our correlation precision with high accuracy, we next used a single fluorescent spot of the fiducial particles as a blind target. The faint green fluorescence signal visible in **Figure 3D**, originating from another z -plane (orthogonal planes depicted with the red lines), belongs to fiducial particles attached to the cell membrane (orthogonal views shown in **Figures 3E,F**). Blind correlation of the signal recorded from this single spot in CSLM, before EM preparation, with the volume EM data, placed the peak of the fluorescence signal 60 nm in X , 90 nm in Y , and 330 nm in Z direction from the center of mass of the two fiducial particles. This indicates that we can reach a correlation accuracy of sub-100 nm in the XY dimension and sub-350 nm in the Z direction.

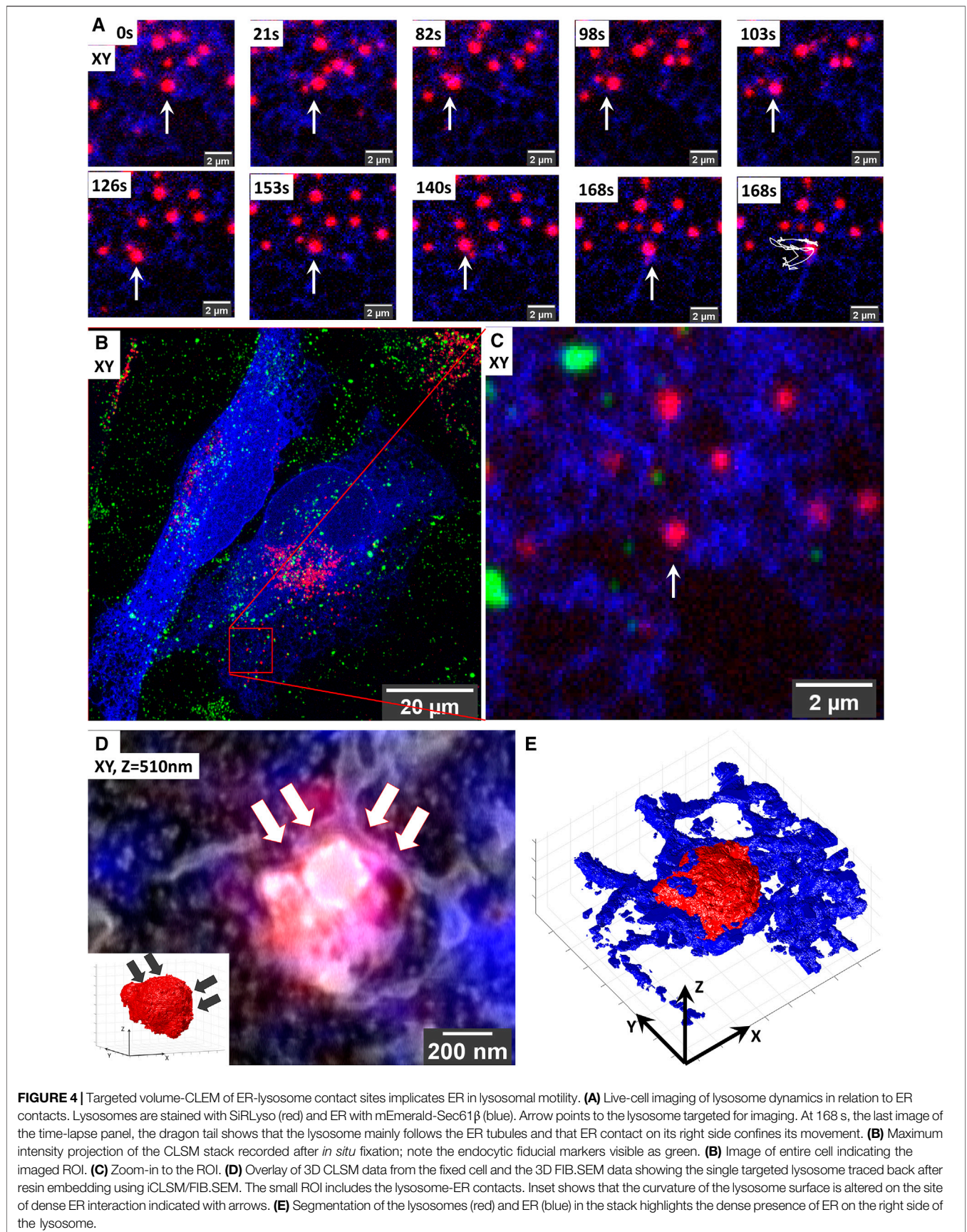
Together these data show that our high-precision volume-CLEM approach allows targeting single organelles identified by CLSM, which within 1–2 h can be correlated, targeted, and imaged in volume EM with 100 nm confidence. This reliable targeted imaging approach greatly improves the throughput of the volume EM technique.

3.4 Targeted Volume-CLEM Efficiently Reveals Inter-Organelle Contact Sites

The possibility of rapid, targeted volume-CLEM with <100 nm precision opens new avenues for imaging at sub-organelle scale (e.g., organelle subdomains), as well as the correlation of rare or transient structures in cells. As an illustration for this application, we examined membrane contact sites (MSCs) between lysosomes and ER. Organelles can communicate with each other by vesicular traffic and MCSs, by which membranes are closely positioned and tethered, but there is no fusion. This special case of intracellular communication facilitates metabolic channeling between distinct (not homotypic) organelles. MSCs between ER and lysosomes mediate the exchange of signaling molecules, ions, metabolites, and lipids, which is important for endo-lysosome maturation and positioning (Friedman et al., 2013; Hönscher et al., 2014; Jongasma et al., 2016; Wijdeven et al., 2016). Only recently, the importance of MSCs in cell physiology was fully recognized, which has made them a focus of attention in contemporary cell biology studies (Phillips and Voeltz, 2015; Wu et al., 2018). However, studying MSCs with high spatial and temporal resolution remains a challenge because of their small size and transient and confined nature. ER-lysosome MSCs are identified as closely apposed (<20 nm) membranes over a distance of 20 nm (Scorrano et al., 2019; Huang et al., 2020). Hence, (3D) EM is essential to provide sufficient resolution to examine the presence and structure of these inter-organelle contacts. However, finding MSCs by EM is akin to seeking a needle in the haystack. We employ our targeted imaging pipeline to efficiently identify MSCs between ER and lysosomes in live cells and visualize their corresponding ultrastructure in 3D (**Figure 4**).

We started this experiment in live cells in which we imaged a single lysosome (SiRLyso) over 3 min for contact moments with ER (mEmerald-Sec61 β) (**Figure 4**). In (live-cell) FM, even though the images are diffraction-limited and it is not possible to make a direct conclusion, all lysosomes appear to have contact with ER. As shown in **Figure 4A**, the targeted lysosome exhibits a diffusive movement. First, it moves toward the left following the ER tubules (**Figure 4A**, 21–98 s); then, it turns right but stops at a blockade formed by ER (**Figure 4A**, 98–103 s). After that, it turns left again and repeats this pattern (live-cell **Supplementary Video S4**). **Figures 4B,C** show the maximum intensity projection of the Z -stack. This analysis suggests that the dense ER visible on the right side of the lysosome defines a confined region for limited movement.

We then prepared the live-cell imaged cell for EM and imaged the particular lysosome-ER interaction site following our targeted imaging pipeline. This high-accuracy targeting is achieved without fiducial particles present in the targeted lysosome (**Figure 4C**). With the high confidence provided by our



method, we could target an ROI of only 1.7 μm wide (**Figure 4D**) and collected 3D ultrastructural data in as little as 190 min between iCSLM and FIB.SEM (with voxels of $1.7 \times 1.7 \times 10$ nm and a dwell time of 10 μs). Note the extremely small size of the imaged ROI compared to the CLSM field of view (132.45 μm wide) (**Figures 4B,C**).

As presented in **Figure 4D**, the 3D-EM identified the targeted organelle as a lysosome with heterogeneous content, including electron-dense material and irregularly organized internal membranes (3D-overlay, **Supplementary Video S5**). Its size is $0.66 \times 0.69 \times 0.50$ μm . Importantly, the 3D-EM data showed that, at its right side, the targeted lysosome is fully covered with the ER cisternae, which follow the limiting membrane of the lysosome, conforming to its shape (**Figure 4E**; 3D-segmentation, **Supplementary Videos S6, S7**). On its left side, we only found tips of ER cisterna touching the lysosome in a poking fashion. The ER on the left side showed a thin tubular lumen, whereas the right-sided ER, which had a blocking effect on lysosome movement, exhibits a sheet-like thicker lumen (**Figure 4D**). Interestingly, the curvature of the lysosome on the right side has a low convexity compared to its highly convex left site (inset, **Figure 4D**), indicating the role of ER contacts also on the shape and possibly composition of lysosome membrane domains. These data show that ER forms multiple types of contact sites with lysosomes, possibly with different functions, which, in addition to the exchange of biomaterials, also defines lysosomal shape and movements. With this example, we prove that our targeted CLEM approach provides a powerful tool to study MSCs from live cells to 3D EM, with high temporal and spatial resolution and a short processing time thanks to optimal ROI selection.

3.5 Volume-CLEM of Multiple Interacting Organelles Followed Over Time

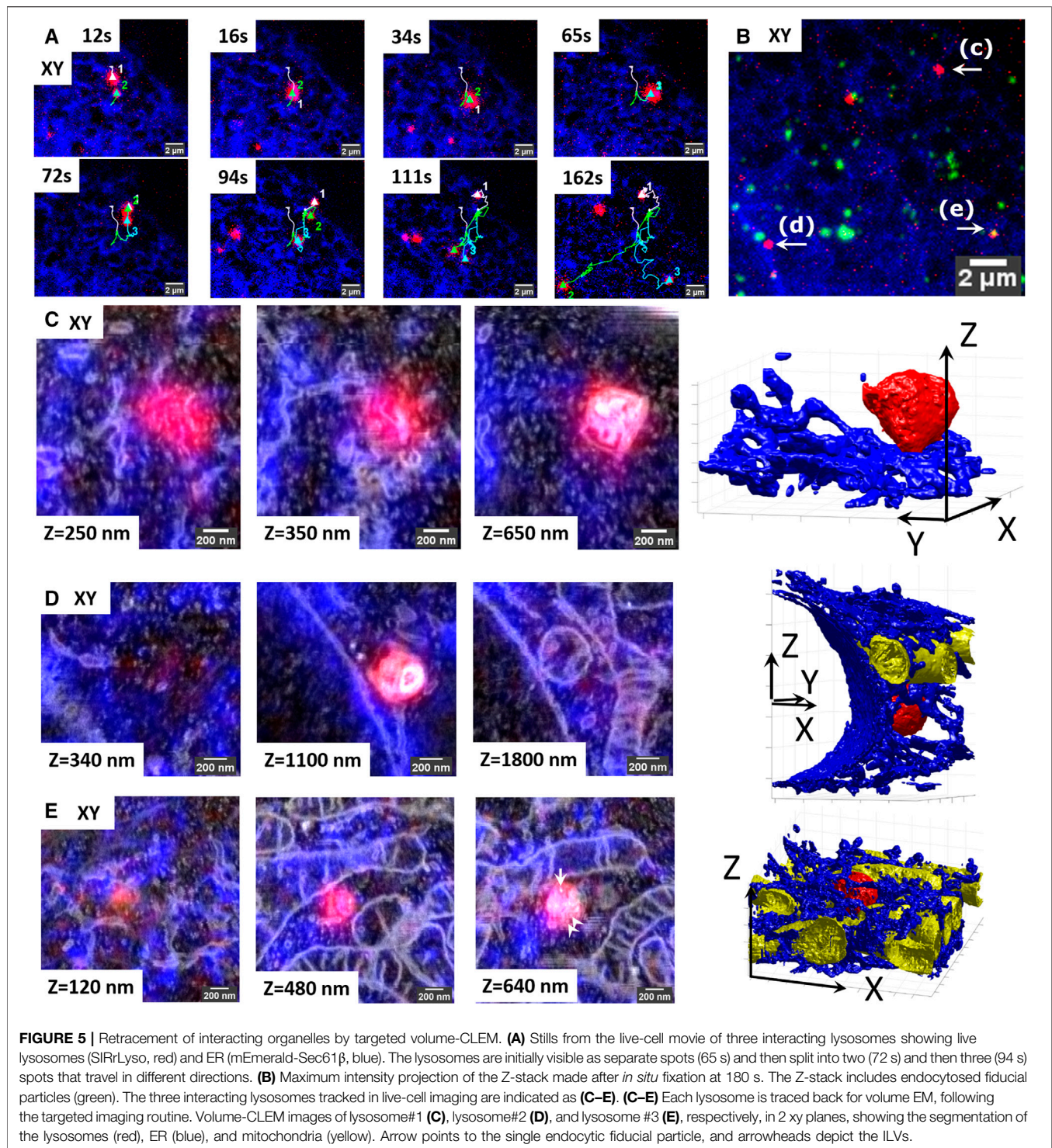
Lysosomes receive input from the endocytic, autophagic, phagocytic, and trans-Golgi network pathways while they traffic throughout the cell (Saftig and Klumperman, 2009). They interact with other lysosomes and endosomes *via* kiss-and-run events or membrane fusion, resulting in the exchange of membranes and content (Huotari and Helenius, 2011; Pols et al., 2013; Jongasma et al., 2020). Although the essential features of lysosomal fusion events have been biochemically established, we do not yet comprehend the spatial and temporal regulation of these processes (Spang, 2016; Ferguson, 2018; van der Beek et al., 2019) simply because there is currently no means to analyze the ultrastructural background of multiple interacting lysosomes in an efficient way and 3D. The targeted volume-CLEM pipeline tackles this challenge by allowing analysis of interactions between multiple, dynamic organelles over time, both in live cells and by EM.

To demonstrate proof-of-principle for this application, we traced three interacting lysosomes over a period of 162 s (**Figure 5**), using the same experimental setup as in the previous experiments (lysosomes stained with SiRLyso, ER with mEmerald-Sec61 β). The larger size lysosome#1 and

relatively smaller lysosome#2 meet at 12 s and traffic a short range together until 65 s. At 72 s, lysosome#3 becomes visible, and all three organelles move through separate tracks between 94 and 162 s (**Figure 5A**). They all stop moving between 162 and 180 s (**Figure 5B**; see also live-cell **Supplementary Video S8**). The movement of lysosome#1 is short-ranged and diffusive, whereas the movements of lysosomes #2 and #3 are long-ranged and directional, indicating microtubule-based transport. Whether these lysosomes just interact or partially fuse during the course of live imaging is not possible to distinguish by FM. Lysosome#1 and lysosome#2 lack endocytic fiducials, whereas lysosome#3 displays a fluorescent signal from the fiducial particles (**Figure 5B**). After EM preparation, we used the position information of the fiducials to trace an extremely small volume across the cell (**Figures 5C–E**), in which we targeted three ROIs, each containing 1 identified lysosome, one by one. Each ROI is approximately 2×2 μm (x, y) in size ($1.55 \times 1.86 \times 0.98$ μm , $1.73 \times 1.68 \times 2.98$ μm , and $2.16 \times 2.24 \times 1.24$ μm exactly), and it required a little over 1 h (64, 68, and 96 min) to collect the complete FIB.SEM datasets. Therefore, within approximately 4 h, we collected three distinct FIB.SEM datasets around three targeted lysosomes that, by live-cell imaging, were seen to interact.

Upon ultrastructural examination and segmentation of the FIB.SEM data, lysosome#1 (red) was found to have a size of $0.56 \times 0.56 \times 0.51$ μm x, y, z , with an asymmetrical shape, positioned at the cell rim between the ER (blue) and the plasma membrane. It had little interactions with ER (blue) (**Figure 5C**, see also 3D-overlay **Supplementary Video S9** and 3D-segmentation **Supplementary Videos S10, S11**). Lysosome#2 (red) had a diameter of $0.55 \times 0.58 \times 0.62$ μm , with a rather spherical shape, positioned in the perinuclear region, touching the nuclear envelope and making contact with a mitochondrion (yellow) and occasional ER tubules (blue). Its luminal content with degraded membranes was comparable to lysosome#1 (**Figure 5D**, see also 3D-overlay **Supplementary Video S12**; 3D-segmentation **Supplementary Video S13**). Lastly, lysosome#3 (red) had a diameter of $0.49 \times 0.53 \times 0.46$ μm x, y, z , with an almost spherical shape, positioned in mitochondria and ER-rich region so dense that the 3D representation became difficult (**Figure 5E**, see also 3D-overlay **Supplementary Video S14**; 3D-segmentation **Supplementary Video S15**). Lysosome#3 was completely surrounded by mitochondria, which may explain its block in movement between 162 and 180 s. In contrast to lysosomes #1 and #2, lysosome #3 contains less electron-dense material, multiple ILVs (arrowheads), and a single endocytic fiducial particle (arrow, bright spot), defining it as late endosome rather than lysosome.

These data show that targeted volume-CLEM provides a fast and feasible method to study time-resolved interactions between multiple organelles and with high resolution. When combined with overexpression or depletion of specific cargo or transport machinery proteins, this approach will provide a unique way to link molecular regulation to transport dynamics and organelle positioning.



4 DISCUSSION

Herein, we have established a volume-CLEM pipeline to correlate every organelle imaged in live cells to volume EM with high-throughput and high-precision. We reached this by bringing together recent developments in integrated CLEM instrumentation using an integrated CLSM-FIB/SEM, novel

endocytic fiducial markers that remain fluorescent in resin embedded samples (Fokkema et al., 2018), and advances in sample preparation that minimize resin embedding (Schieber et al., 2017; van Donselaar et al., 2018). Using 3D z-stacks of endocytic fiducial particles as a 3D coordinate anchor between stand-alone CLSM and integrated CLSM platforms, we match the coordinate planes between 3D-FM and 3D-EM modalities and

identify exact coordinates for each organelle imaged in live-cell FM back in volume EM by FIB-SEM. In **Figure 2**, we show the direct correlation of live-cell imaging data of hydrolase active lysosomes and ER to volume EM data with a correlation precision far below the x , y , z resolution limits of the FM.

We succeeded in achieving the <100 nm sub-organelle level correlation accuracy between 3D-FM and 3D-EM datasets using only a few endocytosed fiducial particles, which function as anchor points between 3D FM and 3D EM. Importantly, correlation is not limited to organelles bearing fiducial particles. Furthermore, other fluorescence signals lost after EM embedding can be correlated to the volume EM data with high precision, using the fiducials as landmarks. Hence, we are not hindered in our EM analysis by the presence of abundant quantities of the fiducial marker. To realize this, we used Au core-silica shell particles recently developed in our labs, which preserve their fluorescence in epoxy resin (Fokkema et al., 2018). Other fiducial particles with the same properties (Kukulski et al., 2012; Takizawa et al., 2015; Han et al., 2019) are equally suited for our approach. Moreover, other fluorescent probes (Morrison et al., 2015; Paez-Segala et al., 2015; Hemelaar et al., 2017; Fu et al., 2020; Tanida et al., 2020), sample preparation routines (Peddie et al., 2014; Brama et al., 2015; Hohn et al., 2015; Andrian et al., 2020), and resins (Zhou et al., 2017) developed to retain the available fluorescence signal after EM sample preparation can be adapted and used within the here described pipeline, using fiducials as correlation anchor.

Precise correlation with *a priori* information from live-cell and confocal FM provides exact 3D coordinates of structures within the complete block and enables targeting for volume EM. In **Figure 3**, we show targeted volume-CLEM (i.e., using the FM identified coordinates to target the ROI in EM) of a single lysosome within the whole cell volume. Blind assessment of the 3D correlation accuracy showed that we could target a single point with sub-100 nm accuracy in the x , y direction and ~300 nm accuracy in the Z direction. Hence, an ROI identified in CLSM can be correlated, targeted, and imaged in volume EM with at least 100 nm confidence. This enables 3D EM visualization of a single organelle (e.g., the lysosome tracked in **Figure 3**) in a notably short time (~2.5 h) and directly correlating to the corresponding FM data. Also addressing homotypic organelle interactions, we investigated prolonged interactions of three lysosomes in live cells in **Figure 5**. Subsequent FIB-SEM of each three lysosomes one by one was completed in less than 4 h, highlighting the novel means that targeted volume-CLEM pipeline offers to analyze the ultrastructure of previously interacted organelles in a high throughput manner.

High-throughput volume-CLEM, including time-resolved functional imaging in live cells, opens up novel possibilities to study the regulation of rare, transient cellular processes with ultrastructural resolution. An extensive understanding of MCSs has been uncovered in the last years presented as one of our examples. In **Figure 4**, we provide the first direct evidence that ER-lysosome contacts regulate lysosome movement and shape in 3D with high temporal and spatial resolution. We analyzed the motility of a single lysosome with respect to its interactions with ER in live cells and visualized that the lysosome movements

mainly follow the surrounding ER tubules. Interaction with dense (bright) ER on one (right) side seemed to obstruct its movement. Once tracked and imaged in volume EM, we showed that the non-obstructive ER at the left-side ER showed a thin tubular lumen, which only touches the lysosome. In contrast, dense ER on the obstacle-side exhibits a sheet-like thicker lumen and wraps the lysosome surface. Interestingly, the curvature of the lysosome on the ER wrapped site was much flatter than its left site (**Figure 4D**), indicating a role of ER contacts in shape and possibly composition of lysosome membrane domains. The data also confirmed the presence of multiple types of contact sites between ER and lysosomes, possibly with different functions (Garrity et al., 2016; Bonifacino and Neefjes, 2017; Fermie et al., 2018; Lim et al., 2019). Numerous proteins involved in MCSs are currently being identified, and many studies focus on addressing the role of these proteins in the spatial and temporal regulation of MCSs at the molecular level (Lim et al., 2019; Cabukusta et al., 2020; Huang et al., 2020). We believe our method, uniquely linking live-cell imaging of single organelles to ultrastructural detail, is promising to greatly accelerate understanding in temporal and structural regulation of MCSs at the system and molecular level.

Besides organelle biology, other fields of cell and developmental biology, model organism studies, and clinical studies can also benefit from our novel, targeted volume-CLEM pipeline. A specific development stage in a model organism, a specific cell within an organoid, and a certain cell cycle stage can be selected by live-cell imaging to address the ultrastructural changes in, for example, cellular differentiation, mechanisms of cellular polarization, and cytokinesis at the nanometer scale. High-precision correlation of 3D-FM and 3D-EM data will allow the use of 3D culture models (e.g., spheroids, organoids) in high-throughput volume-CLEM, which is currently far from trivial (Ando et al., 2018; Rios and Clevers, 2018).

Any fluorescence/light microscopy technique can be incorporated prior to EM sample preparation in the presented volume-CLEM pipeline. We have presented live-cell imaging and confocal FM, forming the foundation for other FM techniques. Specialized fluorescence methods to study organelle dynamics and membrane trafficking (FRAP), transient molecular interactions (FRET), and local exponential fluorescence decay rates in a sample (FLIM) can be directly incorporated within the workflow (De Los Santos et al., 2015) and also super-resolution techniques to study subcellular structures with greater temporal and/or spatial resolution (Hell et al., 2015; Schermelleh et al., 2019). The registration accuracy is currently limited by the FM resolution, and the volume-CLEM pipeline would clearly benefit from the improved lateral and axial resolution, that a super-resolution FM technique could provide (Shtengel et al., 2014; Fu et al., 2020). Similarly, the fluorescence labeling strategies can be adapted to include any types of fluorescent probes, functional reporters (as shown by SiRlyso), fluorescent proteins (as shown by mEmerald), and inorganic dyes (as shown by Rhodamine in fiducial particles). The targeted volume-CLEM pipeline is, therefore, fully flexible in terms of light microscopy approaches.

The targeted imaging strategy reported here would also be very beneficial in uniting with another exciting EM technique, cryo-electron tomography (cryo-ET) to aid cryo-CLEM workflows. These workflows include freezing the cells or tissues, first imaging them in cryo-FM to identify ROI, then transferring them to cryo-FIB.SEM to prepare lamella from the selected ROI (selected Z-plane), and then finally transferring them to the cryo-TEM to acquire the series of 2D images creating the 3D model. Even though being enormously powerful for studying cellular and molecular interactions *in situ* with unmatched resolution, this method is very laborious, low throughput, and available to a limited number of groups in the world. The targeted imaging approach would also solve the main bottleneck also present in these approaches by increasing accuracy and throughput. Implementing a similar iCLSM in a cryo-FIB.SEM setup would assure the lamella preparation of the correct plane, bearing the ROI, for follow-up cryo-TEM imaging. This would unlock the true potential of cryo-CLEM to identify and study rare cellular processes *in situ*, with molecular resolution. Such integrated platforms are currently being commercialized (e.g., METEOR, Delmic).

Structure-function studies of (sub)cellular events require quantitative analyses, which necessitate repetitive imaging of smaller volumes from several independent samples. The targeted volume EM imaging presented herein is a powerful way to find back a small ROI within a large sample. This is especially relevant in a disruptive technique, such as FIB.SEM, and very important to unveil the true quantitative potential of volume EM, which we are just starting to fully utilize (Lucas et al., 2012; Peddie and Collinson, 2014; Hoffman et al., 2020). Another related asset of the targeted imaging approach presented here is the time and resource savings it provides. Usually, imaging a full mammalian cell with 5 nm isotropic resolution in FIB.SEM takes 5–7 days, whereas most of the cell volume does not contain relevant information on the dedicated research question. In contrast, our targeted volume-CLEM pipeline can identify, target, and image an ROI guaranteed to address the research question within 1–2 h, with high confidence. The reduced EM imaging duration saves both personnel and machine time, which is crucial for instruments such as FIB.SEMs often shared by multiple users in imaging facilities. It also considerably cuts back on the post-collection computational requirements of alignment, reconstruction, and segmentation of large 3D-EM datasets (e.g., of whole cells) and the possible correlation with the FM data, which can take as long as the experiment itself. The time for targeting, imaging, and correlation could be further shortened by integrating iCLSM and EM operating software [e.g., SBEM image

(Titze et al., 2018), MAPS/Thermo Fischer, Atlas/Zeiss, ODEMIS/Delmic]. In addition, precise 3D-FM to 3D-EM correlation can facilitate automated image processing and provide ground truth for ongoing efforts on automatized segmentation of 3D-EM datasets (Xiao et al., 2018). Together, these will enable fast and user-independent quantification (e.g., volume and membrane interactions) of structures of interest in significant sample sizes.

DATA AVAILABILITY STATEMENT

The original contributions presented in the study are included in the article/**Supplementary Material**, further inquiries can be directed to the corresponding author.

AUTHOR CONTRIBUTIONS

NL, SL, JFe, HG and JK designed the study. JFe performed the cell culture, labeling, live-cell imaging, and confocal microscopy and analyzed the data with NL. JFo synthesized, characterized, and provided the endocytic fiducials. JFe and CdeH optimized and performed EM sample preparation. SL, AA, GB and HG designed and built the integrated CLSM. SL performed integrated CLSM and FIB.SEM imaging and analyzed the data with NL. SL did the 3D image correlation and segmentation and prepared the figures with NL. NL and SL wrote the paper with input from all authors. HG and JK reviewed the manuscript.

FUNDING

This work was supported by funding from Stichting voor de Technische Wetenschappen (STW), grant number 12715, granted to HG and JK. NL also acknowledges the Netherlands Organization for Scientific Research (NWO) for an ZonMW-TOP grant (91216006) awarded to JK. The authors also acknowledge NWO roadmap grant, The Netherlands Electron Microscopy Infrastructure (NEMI) chaired by JK.

SUPPLEMENTARY MATERIAL

The Supplementary Material for this article can be found online at: <https://www.frontiersin.org/articles/10.3389/fcell.2022.829545/full#supplementary-material>

REFERENCES

- Ando, T., Bhamidimarri, S. P., Brending, N., Colin-York, H., Collinson, L., De Jonge, N., et al. (2018). The 2018 Correlative Microscopy Techniques Roadmap. *J. Phys. D: Appl. Phys.* 51, 443001. doi:10.1088/1361-6463/aad055
- Andrian, T., Bakkum, T., van Elsland, D. M., Bos, E., Koster, A. J., Albertazzi, L., et al. (2020). Super-resolution Correlative Light-Electron Microscopy Using a Click-Chemistry Approach for Studying Intracellular Trafficking. *Methods Cel Biol.* 162, 303–331. doi:10.1016/bs.mcb.2020.09.001
- Ballabio, A., and Bonifacino, J. S. (2019). Lysosomes as Dynamic Regulators of Cell and Organismal Homeostasis. *Nat. Rev. Mol. Cel Biol.* 21, 101–118. doi:10.1038/s41580-019-0185-4
- Blazques-Llorca, L., Hummel, E., Zou, C., Burgold, S., Rietdorf, J., and Herms, J. (2015). Correlation of Two-Photon *In Vivo* Imaging and FIB/SEM Microscopy. *J. Microsc.* 259, 129–136. doi:10.1111/jmi.12231

- Bonifacino, J. S., and Neefjes, J. (2017). Moving and Positioning the Endolysosomal System. *Curr. Opin. Cell Biol.* 47, 1–8. doi:10.1016/j.ccb.2017.01.008
- Brama, E., Peddie, C. J., Jones, M. L., Domart, M. C., Snetkov, X., Way, M., et al. (2015). Standard Fluorescent Proteins as Dual-Modality Probes for Correlative Experiments in an Integrated Light and Electron Microscope. *J. Chem. Biol.* 8, 179–188. doi:10.1007/s12154-015-0143-3
- Brama, E., Peddie, C. J., Wilkes, G., Gu, Y., Collinson, L. M., and Jones, M. L. (2016). miniLM: ultraLM and miniLM: Locator Tools for Smart Tracking of Fluorescent Cells in Correlative Light and Electron Microscopy. *Wellcome Open Res.* 1, 26. doi:10.12688/wellcomeopenres.10299.1
- Burel, A., Lavault, M. T., Chevalier, C., Gnaegi, H., Prigent, S., Mucciolo, A., et al. (2018). A Targeted 3D EM and Correlative Microscopy Method Using SEM Array Tomography. *Development* 145, dev160879. doi:10.1242/dev.160879
- Bushby, A. J., P'ng, K. M. Y., Young, R. D., Pinali, C., Knupp, C., and Quantock, A. J. (2011). Imaging Three-Dimensional Tissue Architectures by Focused Ion Beam Scanning Electron Microscopy. *Nat. Protoc.* 6, 845–858. doi:10.1038/nprot.2011.332
- Butkevich, A. N., Lukinavičius, G., D'Este, E., and Hell, S. W. (2017). Cell-Permeant Large Stokes Shift Dyes for Transfection-free Multicolor Nanoscopy. *J. Am. Chem. Soc.* 139, 12378–12381. doi:10.1021/jacs.7b06412
- Cabukusta, B., Berlin, I., van Elsland, D. M., Forkink, I., Spits, M., de Jong, A. W. M., et al. (2020). Human VAPome Analysis Reveals MOSPD1 and MOSPD3 as Membrane Contact Site Proteins Interacting with FFAT-Related FFNT Motifs. *Cell Rep* 33, 108475. doi:10.1016/j.celrep.2020.108475
- Cabukusta, B., and Neefjes, J. (2018). Mechanisms of Lysosomal Positioning and Movement. *Traffic* 19, 761–769. doi:10.1111/tra.12587
- Collinson, L. M., Carroll, E. C., and Hoogenboom, J. P. (2017). Correlating 3D Light to 3D Electron Microscopy for Systems Biology. *Curr. Opin. Biomed. Eng.* 3, 49–55. doi:10.1016/j.cobme.2017.10.006
- Collman, F., Buchanan, J., Phend, K. D., Micheva, K. D., Weinberg, R. J., and Smith, S. J. (2015). Mapping Synapses by Conjugate Light-Electron Array Tomography. *J. Neurosci.* 35, 5792–5807. doi:10.1523/jneurosci.4274-14.2015
- De Los Santos, C., Chang, C.-W., Mycek, M.-A., and Cardullo, R. A. (2015). FRAP, FLIM and FRET: Detection and Analysis of Cellular Dynamics on a Molecular Scale Using Fluorescence Microscopy. *Mol. Reprod. Dev.* 82, 587–604. doi:10.1002/mrd.22501
- Delpiano, J., Pizarro, L., Peddie, C. J., Jones, M. L., Griffin, L. D., and Collinson, L. M. (2018). Automated Detection of Fluorescent Cells in In-Resin Fluorescence Sections for Integrated Light and Electron Microscopy. *J. Microsc.* 271, 109–119. doi:10.1111/jmi.12700
- Denk, W., and Horstmann, H. (2004). Serial Block-Face Scanning Electron Microscopy to Reconstruct Three-Dimensional Tissue Nanostructure. *PLoS Biol.* 2, e329. doi:10.1371/journal.pbio.0020329
- Fang, T., Lu, X., Berger, D., Gmeiner, C., Cho, J., Schalek, R., et al. (2018). Nanobody Immunostaining for Correlated Light and Electron Microscopy with Preservation of Ultrastructure. *Nat. Methods* 15, 1029–1032. doi:10.1038/s41592-018-0177-x
- Ferguson, S. M. (2018). Axonal Transport and Maturation of Lysosomes. *Curr. Opin. Neurobiol.* 51, 45–51. doi:10.1016/j.conb.2018.02.020
- Ferguson, S. M. (2019). Neuronal Lysosomes. *Neurosci. Lett.* 697, 1–9. doi:10.1016/j.neulet.2018.04.005
- Fermie, J., Liv, N., ten Brink, C., van Donselaar, E. G., Müller, W. H., Schieber, N. L., et al. (2018). Single Organelle Dynamics Linked to 3D Structure by Correlative Live-Cell - 3D Electron Microscopy. *Traffic* 19, 354–369. doi:10.1111/tra.12557
- Fokkema, J., Fermie, J., Liv, N., van den Heuvel, D. J., Konings, T. O. M., Blab, G. A., et al. (2018). Fluorescently Labelled Silica Coated Gold Nanoparticles as Fiducial Markers for Correlative Light and Electron Microscopy. *Sci. Rep.* 8, 13625. doi:10.1038/s41598-018-31836-1
- Friedman, J. R., Dibeneditto, J. R., West, M., Rowland, A. A., and Voeltz, G. K. (2013). Endoplasmic Reticulum-Endosome Contact Increases as Endosomes Traffic and Mature. *MBoC* 24, 1030–1040. doi:10.1091/mbc.e12-10-0733
- Fu, Z., Peng, D., Zhang, M., Xue, F., Zhang, R., He, W., et al. (2020). mEosEM Withstands Osmium Staining and Epon Embedding for Super-resolution CLEM. *Nat. Methods* 17, 55–58. doi:10.1038/s41592-019-0613-6
- Garrity, A. G., Wang, W., Collier, C. M. D., Levey, S. A., Gao, Q., and Xu, H. (2016). The Endoplasmic Reticulum, Not the pH Gradient, Drives Calcium Refilling of Lysosomes. *Elife* 5, e15887. doi:10.7554/eLife.15887
- Gatta, A. T., and Levine, T. P. (2016). Piecing Together the Patchwork of Contact Sites. *Trends Cell Biol.* 20, 359–366. doi:10.1016/j.tcb.2016.08.010
- Gorelick, S., Buckley, G., Gervinskas, G., Johnson, T. K., Handley, A., Caggiano, M. P., et al. (2019). PIE-scope, Integrated Cryo-Correlative Light and FIB/SEM Microscopy. *Elife* 8, e45919. doi:10.7554/eLife.45919
- Han, S., Raabe, M., Hodgson, L., Mantell, J., Verkade, P., Lasser, T., et al. (2019). High-Contrast Imaging of Nanodiamonds in Cells by Energy Filtered and Correlative Light-Electron Microscopy: Toward a Quantitative Nanoparticle-Cell Analysis. *Nano Lett.* 19, 2178–2185. doi:10.1021/acs.nanolett.9b00752
- Hell, S. W., Sahl, S. J., Bates, M., Zhuang, X., Heintzmann, R., Booth, M. J., et al. (2015). The 2015 Super-resolution Microscopy Roadmap. *J. Phys. D: Appl. Phys.* 48, 443001. doi:10.1088/0022-3727/48/44/443001
- Hemelaar, S. R., de Boer, P., Chipaux, M., Zuidema, W., Hamoh, T., Martinez, F. P., et al. (2017). Nanodiamonds as Multi-Purpose Labels for Microscopy. *Sci. Rep.* 7, 720. doi:10.1038/s41598-017-00797-2
- Heymann, J. A. W., Hayles, M., Gestmann, I., Giannuzzi, L. A., Lich, B., and Subramaniam, S. (2006). Site-specific 3D Imaging of Cells and Tissues with a Dual Beam Microscope. *J. Struct. Biol.* 155, 63–73. doi:10.1016/j.jsb.2006.03.006
- Hoffman, D. P., Shtengel, G., Xu, C. S., Campbell, K. R., Freeman, M., Wang, L., et al. (2020). Correlative Three-Dimensional Super-resolution and Block-Face Electron Microscopy of Whole Vitreously Frozen Cells. *Science* 367, eaaz5357. doi:10.1126/science.aaz5357
- Hohn, K., Fuchs, J., Frober, A., Kirmse, R., Anders-Össwein, M., Walter, P., et al. (2015). Preservation of Protein Fluorescence in Embedded Human Dendritic Cells for Targeted 3D Light and Electron Microscopy. *J. Microsc.* 259, 121–128. doi:10.1111/jmi.12230
- Hönscher, C., Mari, M., Auffarth, K., Bohnert, M., Griffith, J., Geerts, W., et al. (2014). Cellular Metabolism Regulates Contact Sites between Vacuoles and Mitochondria. *Dev. Cell* 30, 86–94. doi:10.1016/j.devcel.2014.06.006
- Huang, X., Jiang, C., Yu, L., and Yang, A. (2020). Current and Emerging Approaches for Studying Inter-organelle Membrane Contact Sites. *Front. Cell Dev. Biol.* 8, 195. doi:10.3389/fcell.2020.00195
- Huotari, J., and Helenius, A. (2011). Endosome Maturation. *EMBO J.* 30, 3481–3500. doi:10.1038/emboj.2011.286
- Jongsma, M. L., Bakker, J., Cabukusta, B., Liv, N., van Elsland, D., Fermie, J., et al. (2020). SKIP-HOPS Recruits TBC1D15 for a Rab7-To-Arl8b Identity Switch to Control Late Endosome Transport. *EMBO J.* 39, e102301. doi:10.15252/embj.2019102301
- Jongsma, M. L. M., Berlin, I., Wijdeven, R. H. M., Janssen, L., Janssen, G. M. C., Garstka, M. A., et al. (2016). An ER-Associated Pathway Defines Endosomal Architecture for Controlled Cargo Transport. *Cell* 166, 152–166. doi:10.1016/j.cell.2016.05.078
- Keene, D. R., Tufa, S. F., Lunstrum, G. P., Holden, P., and Horton, W. A. (2008). Confocal/TEM Overlay Microscopy: A Simple Method for Correlating Confocal and Electron Microscopy of Cells Expressing GFP/YFP Fusion Proteins. *Microsc. Microanal.* 14, 342–348. doi:10.1017/s1431927608080306
- Kizilyaprak, C., Bittermann, A. G., Daraspe, J., and Humbel, B. M. (2014). FIB-SEM Tomography in Biology. *Methods Mol. Biol.* 1117, 541–558. doi:10.1007/978-1-62703-776-1_24
- Knott, G., Marchman, H., Wall, D., and Lich, B. (2008). Serial Section Scanning Electron Microscopy of Adult Brain Tissue Using Focused Ion Beam Milling. *J. Neurosci.* 28, 2959–2964. doi:10.1523/jneurosci.3189-07.2008
- Knott, G., Rosset, S., and Cantoni, M. (2011). Focussed Ion Beam Milling and Scanning Electron Microscopy of Brain Tissue. *JoVE* 1, 2588. doi:10.3791/2588
- Koning, R. I., Raja, A. S., Lane, R. I., Koster, A. J., and Hoogenboom, J. P. (2019). “Integrated Light and Electron Microscopy,” in *Correlative Imaging* (Wiley), 119–135. doi:10.1002/9781119086420.ch7
- Kukulski, W., Schorb, M., Welsch, S., Picco, A., Kaksonen, M., and Briggs, J. A. G. (2012). Precise, Correlated Fluorescence Microscopy and Electron Tomography of Lowicryl Sections Using Fluorescent Fiducial Markers. *Methods Cell Biol.* 111, 235–257. doi:10.1016/b978-0-12-416026-2.00013-3
- Lane, R., de Boer, P., Giepmans, B. N. G., and Hoogenboom, J. P. (2019). Integrated Array Tomography for High Throughput Electron Microscopy. *Microsc. Microanal.* 25, 1038–1039. doi:10.1017/s1431927619005920
- Lim, C. Y., Davis, O. B., Shin, H. R., Zhang, J., Berdan, C. A., Jiang, X., et al. (2019). ER-lysosome Contacts Enable Cholesterol Sensing by mTORC1 and Drive Aberrant Growth Signalling in Niemann-Pick Type C. *Nat. Cell Biol.* 21, 1206–1218. doi:10.1038/s41556-019-0391-5
- Liv, N., Zonneville, A. C., Narvaez, A. C., Efting, A. P. J., Voorneveld, P. W., Lucas, M. S., et al. (2013). Simultaneous Correlative Scanning Electron and High-NA Fluorescence Microscopy. *PLoS One* 8, e55707. doi:10.1371/journal.pone.0055707

- Lucas, M. S., Günthert, M., Gasser, P., Lucas, F., and Wepf, R. (2012). Bridging Microscopes. *Methods Cel Biol* 111, 325–356. doi:10.1016/b978-0-12-416026-2.00017-0
- Lukinavičius, G., Reymond, L., Umezawa, K., Sallin, O., D'Este, E., Göttfert, F., et al. (2016). Fluorogenic Probes for Multicolor Imaging in Living Cells. *J. Am. Chem. Soc.* 138, 9365–9368. doi:10.1021/jacs.6b04782
- Meel, E., and Klumperman, J. (2008). Imaging and Imagination: Understanding the Endo-Lysosomal System. *Histochem. Cel Biol.* 129, 253–266. doi:10.1007/s00418-008-0384-0
- Micheva, K. D., and Smith, S. J. (2007). Array Tomography: A New Tool for Imaging the Molecular Architecture and Ultrastructure of Neural Circuits. *Neuron* 55, 25–36. doi:10.1016/j.neuron.2007.06.014
- Mohammadian, S., Fokkema, J., Agronskaia, A. V., Liv, N., de Heus, C., van Donselaar, E., et al. (2019). High Accuracy, Fiducial Marker-Based Image Registration of Correlative Microscopy Images. *Sci. Rep.* 9, 3211. doi:10.1038/s41598-019-40098-4
- Morrison, I. E. G., Samilian, A., Coppo, P., Ireland, T. G., Fern, G. R., Silver, J., et al. (2015). Multicolour Correlative Imaging Using Phosphor Probes. *J. Chem. Biol.* 8, 169–177. doi:10.1007/s12154-015-0141-5
- Narayan, K., Danielson, C. M., Lagarec, K., Lowekamp, B. C., Coffman, P., Laquerre, A., et al. (2014). Multi-resolution Correlative Focused Ion Beam Scanning Electron Microscopy: Applications to Cell Biology. *J. Struct. Biol.* 185, 278–284. doi:10.1016/j.jsb.2013.11.008
- Nixon-Abell, J., Obara, C. J., Weigel, A. V., Li, D., Legant, W. R., Xu, C. S., et al. (2016). Increased Spatiotemporal Resolution Reveals Highly Dynamic Dense Tubular Matrices in the Peripheral ER. *Science* 354, aaf3928. doi:10.1126/science.aaf3928
- Oberti, D., Kirschmann, M. A., and Hahnloser, R. H. (2011). Projection Neuron Circuits Resolved Using Correlative Array Tomography. *Front. Neurosci.* 5, 50–58. doi:10.3389/fnins.2011.00050
- Paez-Segala, M. G., Sun, M. G., Shtengel, G., Viswanathan, S., Baird, M. A., Macklin, J. J., et al. (2015). Fixation-resistant Photoactivatable Fluorescent Proteins for CLEM. *Nat. Methods* 12, 215–218. doi:10.1038/nmeth.3225
- Peddie, C. J., and Collinson, L. M. (2014). Exploring the Third Dimension: Volume Electron Microscopy Comes of Age. *Micron* 61, 9–19. doi:10.1016/j.micron.2014.01.009
- Peddie, C. J., Liv, N., Hoogenboom, J. P., and Collinson, L. M. (2014). Integrated Light and Scanning Electron Microscopy of GFP-Expressing Cells. *Methods Cel Biol.* 124, 363–389. doi:10.1016/B978-0-12-801075-4.00017-3
- Phillips, M. J., and Voeltz, G. K. (2015). Structure and Function of ER Membrane Contact Sites with Other Organelles. *Nat. Rev. Mol. Cel Biol.* 17, 69–82. doi:10.1038/nrm.2015.8
- Pols, M. S., Ten Brink, C., Gosavi, P., Oorschot, V., and Klumperman, J. (2013). The HOPS Proteins hVps41 and hVps39 Are Required for Homotypic and Heterotypic Late Endosome Fusion. *Traffic* 14, 219–232. doi:10.1111/tra.12027
- Prabhakar, N., Belevich, I., Peurla, M., Heiligenstein, X., Chang, H.-C., Sahlgren, C., et al. (2020). Cell Volume (3D) Correlative Microscopy Facilitated by Intracellular Fluorescent Nanodiamonds as Multi-Modal Probes. *Nanomaterials* 11, 14. doi:10.3390/nano11010014
- Rios, A. C., and Clevers, H. (2018). Imaging Organoids: A Bright Future Ahead. *Nat. Methods* 15, 24–26. doi:10.1038/nmeth.4537
- Ronchi, P., Machado, P., D'Imprima, E., Mizzon, G., Best, B. T., Cassella, L., et al. (2021). Fluorescence-based 3D Targeting of FIB-SEM Acquisition of Small Volumes in Large Samples. *bioRxiv* 1, 427072. doi:10.1101/2021.01.18.427072
- Russell, M. R. G., Lerner, T. R., Burden, J. J., Nkwe, D. O., Pelchen-Matthews, A., Domart, M.-C., et al. (2016). 3D Correlative Light and Electron Microscopy of Cultured Cells Using Serial Blockface Scanning Electron Microscopy. *J. Cel Sci.* 130, 188433. doi:10.1242/jcs.188433
- Saalfeld, S., Cardona, A., Hartenstein, V., and Tomančák, P. (2010). As-rigid-as-possible Mosaicking and Serial Section Registration of Large sSTEM Datasets. *Bioinformatics* 26, i57–63. doi:10.1093/bioinformatics/btq219
- Saftig, P., and Klumperman, J. (2009). Lysosome Biogenesis and Lysosomal Membrane Proteins: Trafficking Meets Function. *Nat. Rev. Mol. Cel Biol.* 10, 623–635. doi:10.1038/nrm2745
- Schermelleh, L., Ferrand, A., Huser, T., Eggeling, C., Sauer, M., Biehlmaier, O., et al. (2019). Super-resolution Microscopy Demystified. *Nat. Cel Biol.* 21, 72–84. doi:10.1038/s41556-018-0251-8
- Schieber, N. L., Machado, P., Markert, S. M., Stigloher, C., Schwab, Y., and Steyer, A. M. (2017). Minimal Resin Embedding of Multicellular Specimens for Targeted FIB-SEM Imaging. *Methods Cel Biol.* 140, 69–83. doi:10.1016/bs.mcb.2017.03.005
- Scorrano, L., De Matteis, M. A., Emr, S., Giordano, F., Hajnóczky, G., Kornmann, B., et al. (2019). Coming Together to Define Membrane Contact Sites. *Nat. Commun.* 10, 1–11. doi:10.1038/s41467-019-09253-3
- Shtengel, G., Wang, Y., Zhang, Z., Goh, W. L., Hess, H. F., and Kanchanawong, P. (2014). Imaging Cellular Ultrastructure by PALM, iPALM, and Correlative iPALM-EM. *Methods Cel Biol.* 123, 273–294. doi:10.1016/b978-0-12-420138-5.00015-x
- Sironi, L., Restelli, L. M., Tolnay, M., Neutzner, A., and Frank, S. (2020). Dysregulated Interorganellar Crosstalk of Mitochondria in the Pathogenesis of Parkinson's Disease. *Cells* 9, 233. doi:10.3390/cells9010233
- Spang, A. (2016). Membrane Tethering Complexes in the Endosomal System. *Front. Cel Dev. Biol.* 4, 35. doi:10.3389/fcell.2016.00035
- Takizawa, T., Powell, R. D., Hainfeld, J. F., and Robinson, J. M. (2015). FluoroNanogold: An Important Probe for Correlative Microscopy. *J. Chem. Biol.* 8, 129–142. doi:10.1007/s12154-015-0145-1
- Tanida, I., Kakuta, S., Oliva Trejo, J. A., and Uchiyama, Y. (2020). Visualization of Cytoplasmic Organelles via In-Resin CLEM Using an Osmium-Resistant Far-Red Protein. *Sci. Rep.* 10, 11314. doi:10.1038/s41598-020-68191-z
- Timmermans, F. J., Liszka, B., Lenferink, A. T. M., van Wolferen, H. A. G. M., and Otto, C. (2016). Integration of Correlative Raman Microscopy in a Dualbeam FIB SEM. *J. Raman Spectrosc.* 47, 956–962. doi:10.1002/jrs.4931
- Titze, B., Genoud, C., and Friedrich, R. W. (2018). SBEMImage: Versatile Acquisition Control Software for Serial Block-Face Electron Microscopy. *Front. Neural Circuits* 12, 54. doi:10.3389/fncir.2018.00054
- van der Beek, J., Jonker, C., van der Welle, R., Liv, N., and Klumperman, J. (2019). CORVET, CHEVI and HOPS - Multisubunit Tethers of the Endo-Lysosomal System in Health and Disease. *J. Cel Sci.* 132, jcs189134. doi:10.1242/jcs.189134
- van Donselaar, E. G., Dorresteyn, B., Popov-čeleketić, D., Van De Wetering, W. J., Verrips, T. C., Boekhout, T., et al. (2018). Extremely Thin Layer Plastification for Focused-Ion Beam Scanning Electron Microscopy: an Improved Method to Study Cell Surfaces and Organelles of Cultured Cells. *J. Microsc.* 270, 359–373. doi:10.1111/jmi.12694
- Weber, I. (2003). [2] Reflection Interference Contrast Microscopy. *Methods Enzymol.* 361, 34–47. doi:10.1016/S0076-6879(03)61004-9
- Wijdeven, R. H., Janssen, H., Nahidiazar, L., Janssen, L., Jalink, K., Berlin, I., et al. (2016). Cholesterol and ORP1L-Mediated ER Contact Sites Control Autophagosomal Transport and Fusion with the Endocytic Pathway. *Nat. Commun.* 7, 11808. doi:10.1038/ncomms11808
- Wong, Y. C., Kim, S., Peng, W., and Krainc, D. (2019). Regulation and Function of Mitochondria-Lysosome Membrane Contact Sites in Cellular Homeostasis. *Trends Cel Biol.* 29, 500–513. doi:10.1016/j.tcb.2019.02.004
- Wu, H., Carvalho, P., and Voeltz, G. K. (2018). Here, There, and Everywhere: The Importance of ER Membrane Contact Sites. *Science* 361, eaan5835. doi:10.1126/science.aan5835
- Xiao, C., Chen, X., Li, W., Li, L., Wang, L., Xie, Q., et al. (2018). Automatic Mitochondria Segmentation for EM Data Using a 3D Supervised Convolutional Network. *Front. Neuroanat.* 12, 92. doi:10.3389/fnana.2018.00092
- Zhou, H., Gang, Y., Chen, S., Wang, Y., and Xiong, Y. (2017). Development of a Neutral Embedding Resin for Optical Imaging of Fluorescently Labeled Biological Tissue. *J. Biomed. Opt.* 22, 1. doi:10.1117/1.jbo.22.10.106015

Conflict of Interest: The authors declare that the research was conducted in the absence of any commercial or financial relationships that could be construed as a potential conflict of interest.

Publisher's Note: All claims expressed in this article are solely those of the authors and do not necessarily represent those of their affiliated organizations or those of the publisher, the editors, and the reviewers. Any product that may be evaluated in this article, or claim that may be made by its manufacturer, is not guaranteed or endorsed by the publisher.

Copyright © 2022 Loginov, Fermie, Fokkema, Agronskaia, De Heus, Blab, Klumperman, Gerritsen and Liv. This is an open-access article distributed under the terms of the Creative Commons Attribution License (CC BY). The use, distribution or reproduction in other forums is permitted, provided the original author(s) and the copyright owner(s) are credited and that the original publication in this journal is cited, in accordance with accepted academic practice. No use, distribution or reproduction is permitted which does not comply with these terms.